A Novel Liquid Adulteration Sensor Based on a Self Complementary Antenna

Jolly Rajendran[1, *], Sreedevi K. Menon[1], and Massimo Donelli[2]

Abstract—In this paper, a novel OLR loaded self complementary dipole antenna (OSCDA) is proposed. Open loop resonators (OLRs) are introduced into the design of a traditional self complementary dipole antenna (SCDA), to evolve it into OSCDA. The antenna is compact and has an impedance bandwidth of 1.1 GHz to 3.3 GHz with VSWR less than 2 across the frequency band. The use of the proposed antenna as a liquid sensor to detect adulteration in liquids is demonstrated from the relationship between concentration and shift in resonant frequency and variation in reflection coefficient. Variation of reflection coefficient due to change in dielectric properties is studied for different cases viz.: (i) dilution of milk with water, (ii) adulteration of coconut oil with rice bran oil, (iii) adulteration of honey with sugar syrup, and (iv) varying concentration of salt and sugar in water. When an adulterant is added to a liquid or concentration of solute in a solution varied, the dielectric properties change. This is reflected in the variation in reflection coefficient and resonant frequency. Experimental results show that the antenna has a good sensitivity to detect adulterated samples.

1. INTRODUCTION

Food adulteration is a common practice to increase profit. Several conventional methods like mid-infrared spectroscopy and chemical methods have been used to detect adulteration [1]. Various methods like pollen analysis [2], stable carbon isotope ratio analysis (SCIRA) [3], liquid chromatography coupled to isotope ratio mass spectrometry [4], gas chromatography-mass spectrometry [5], impedance e-tongue and optical spectroscopy [6], e-noses [7], etc. are used to determine adulteration of honey. Methods like Fatty Acid Methyl Esters (FAME) [8], Quartz Crystal Microbalance (QCM) [9], nuclear magnetic resonance (NMR) fingerprinting [10], e-noses [11], e-tongue [12], etc. are used to detect adulteration in oils. Chemosensing is used to detect the presence of harmful substances in water [13]. All these methods are accurate but are time consuming, expensive, have a comparatively complex procedure, and require a skilled operator. A more cost-effective and simple method for determining the extent of adulteration is required.

Nowadays, microstrip based sensors are widely used as moisture sensors [14], humidity sensors [15], biosensors [16] and to detect salinity of water [17]. Microstrip antennas when being loaded with metamaterial-inspired resonators like Open Loop Resonators (OLRs) and Split Ring Resonators (SRRs) are known to provide a better sensitivity, higher quality factor (Q) and are more compact than ordinary microstrip antenna [18]. These resonators have exotic properties like negative permittivity, negative permeability, negative refractive index, etc. They find application as sensors for detecting temperature [19], detection of protein molecules [20], microfluidic dielectric characterization [21], estimating bone mineral density [22, 23], etc. Wongkasem and Ruiz developed a metamaterial-inspired microfluid microwave sensor using a patch antenna and a microfluidic channel [24]. The principle behind

[1] Department of Electronics and Communication Engineering, Amrita Vishwa Vidyapeetham, Amritapuri, India. [2] Department of Information Engineering and Computer Science, University of Trento, Italy.

such a system is dielectric perturbation phenomenon [24]. When the testing sample is introduced into the sensor system, the electromagnetic boundary conditions change. The resonant frequency shifts due to change in material polarization. Also there is change in Q factor due to the change in dielectric losses in the sample [18].

In this paper, a simple, generalized antenna-based sensor is proposed to detect the adulteration of liquids and the presence of salt and sugar in water. For this, an OLR loaded self complementary dipole antenna (OSCDA) is designed and experimentally assessed, which operates from 1.1 GHz to 3.3 GHz. The obtained results prove that the proposed antenna can function as a liquid sensor. The sensor system is easy to fabricate, simple and is a low cost alternate solution, and it represents a valid tool to detect adulteration.

2. ANTENNA CHARACTERIZATION

The structure of proposed (OSCDA) is reported in Figure 1. It consists of dipole elements bent to form a 'U', in order to reduce the mechanical size. OLRs are placed inside the longer dipoles as shown in Figure 1. The length of dipoles is calculated using the design equations discussed in [25]. The geometric parameters of OSCDA are listed in Table 1, and they have been obtained after an accurate tuning phase aimed at minimizing the VSWR in the whole considered bandwidth. The dipoles are fed by means of a balanced feed line, and a wideband balun is considered to provide the unbalanced to
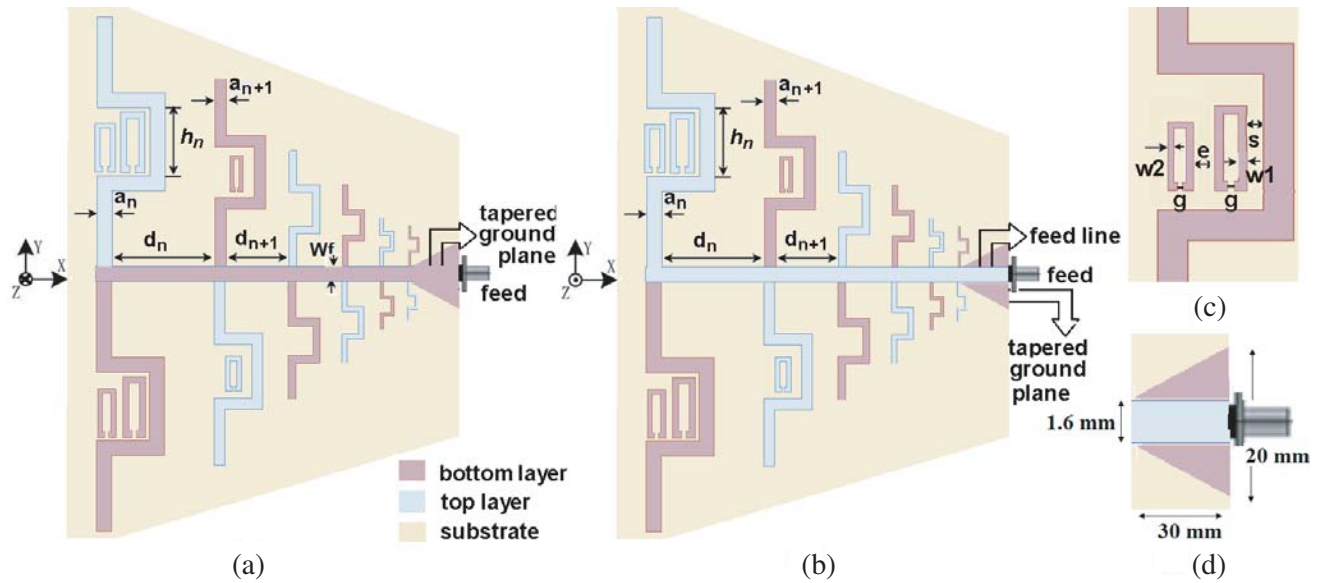

Figure 1. The layout of the OSCDA with geometric parameters. (a) Bottom view. (b) Top view. (c) Layout of a bend dipole loaded with OLRs. (d) The tapered feed line.

Table 1. The geometrical parameters of OSCDA (Dimensions: mm).

n	d_n	a_n	h_n	w_1	s	g	w_2	e
1	23	4	11.5	0.5	0.4	0.3	0.5	1
2	17	3	8.7	0.5	0.3	-	-	-
3	13	2.3	6.6	-	-	-	-	-
4	10	1.7	5.0	-	-	-	-	-
5	8	1.3	3.8	-	-	-	-	-
6	7	1	2.9	-	-	-	-	-

balanced transition [26]. Several baluns like infinite balun [25] or tapered balun [27] are in use. To realize an infinite balun, the outer conductor is soldered to the feed line, which makes the fabrication process and mass production difficult. In the presented design, no external balun is used. Instead, the center feed line is specially designed, which serves the purpose of a wideband balun. This makes the fabrication and mass production easy and also the antenna more compact. In particular, the central feed line is a balanced line with width 1.6 mm. The central feed line is symmetrically tapered to transform a balanced line to unbalanced microstrip line as shown in Figure 1(d). Similar structures are used in microstrip antennas, for wideband matching [27]. The antenna structure has been numerically assessed by means of a commercial electromagnetic simulator namely HFSS. Figure 1(a) and Figure 1(b) display the top and bottom views of the OSCDA configuration and the different parameters of OSCDA. An antenna prototype has been fabricated with a photolithographic technique. The prototype has been equipped with a subminiature type A coaxial connector. The antenna is fabricated on a 1.6 mm thick substrate with $\epsilon_r = 4.4$ and loss tangent $\tan \delta = 0.002$. Figure 2(a) depicts a photo of the fabricated OSCDA prototype.
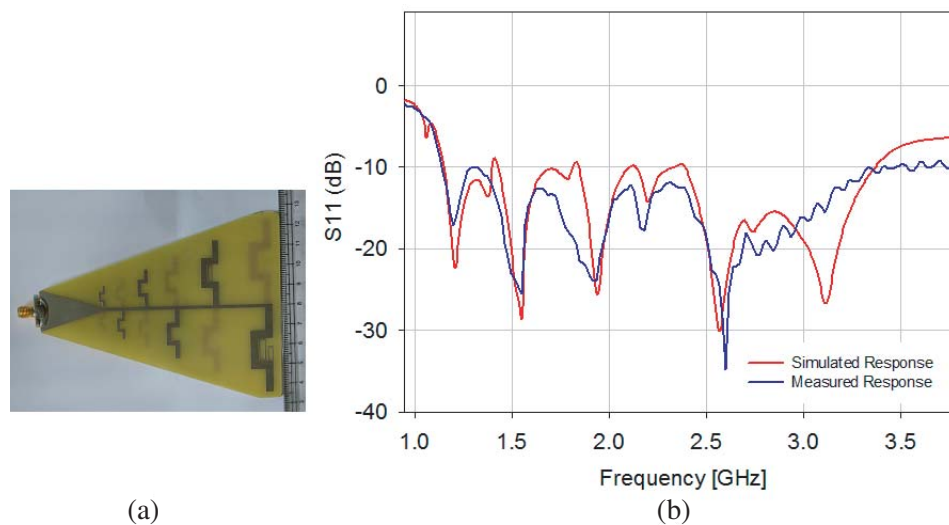

(a)   (b)

Figure 2. (a) The fabricated antenna prototype. (b) The frequency response of S_{11} of OSCDA.

OSCDA can be regarded as a capacitively loaded transmission line. Thus its input impedance is governed by the characteristic impedance of the central balanced feed line [15]. A good impedance match is obtained when the central feed width is 1.6 mm. Figure 2(b) reveals the simulated reflection coefficient which agrees well with the measured ones (measured using Keysight E8050 vector network analyzer). The reflection coefficient is under -10 dB in the frequency range 1.1 GHz to 3.3 GHz, indicating a good wideband impedance matching. The measured response slightly varies from the simulated one due to fabrication tolerances, the variations of substrate permittivity with frequency, and mechanical tolerances. Incorporation of an OLR is found to slightly enhance the bandwidth to a few 100 MHz, with a small shift in the resonant frequency band.

The active region of the antenna is composed of those dipoles whose length is roughly a half wavelength at a certain frequency and the portion of feed line to which the dipoles are attached. The active region is the one that converts the transmission wave to the radiated field. The characteristics of the field that is radiated are determined by the active region, which shifts with frequency. This can be observed from the surface current density plot shown in Figures 3(a)–(f). As can be noticed at lower frequencies, large surface currents are seen at larger dipoles. As the frequency increases, the shorter dipoles have a larger current density. At each resonance, the corresponding half wavelength dipole shows the maximum current density. At 3 GHz, the smallest dipole shows the maximum current density.

The radiation patterns are measured in an anechoic chamber using Agilent E8362B PNA network analyzer giving a continuous sweep of frequencies. OSCDA has a directional pattern. As stated by Floquet wave expansion and spatial harmonic theory, radiation from the OSCDA must be directed
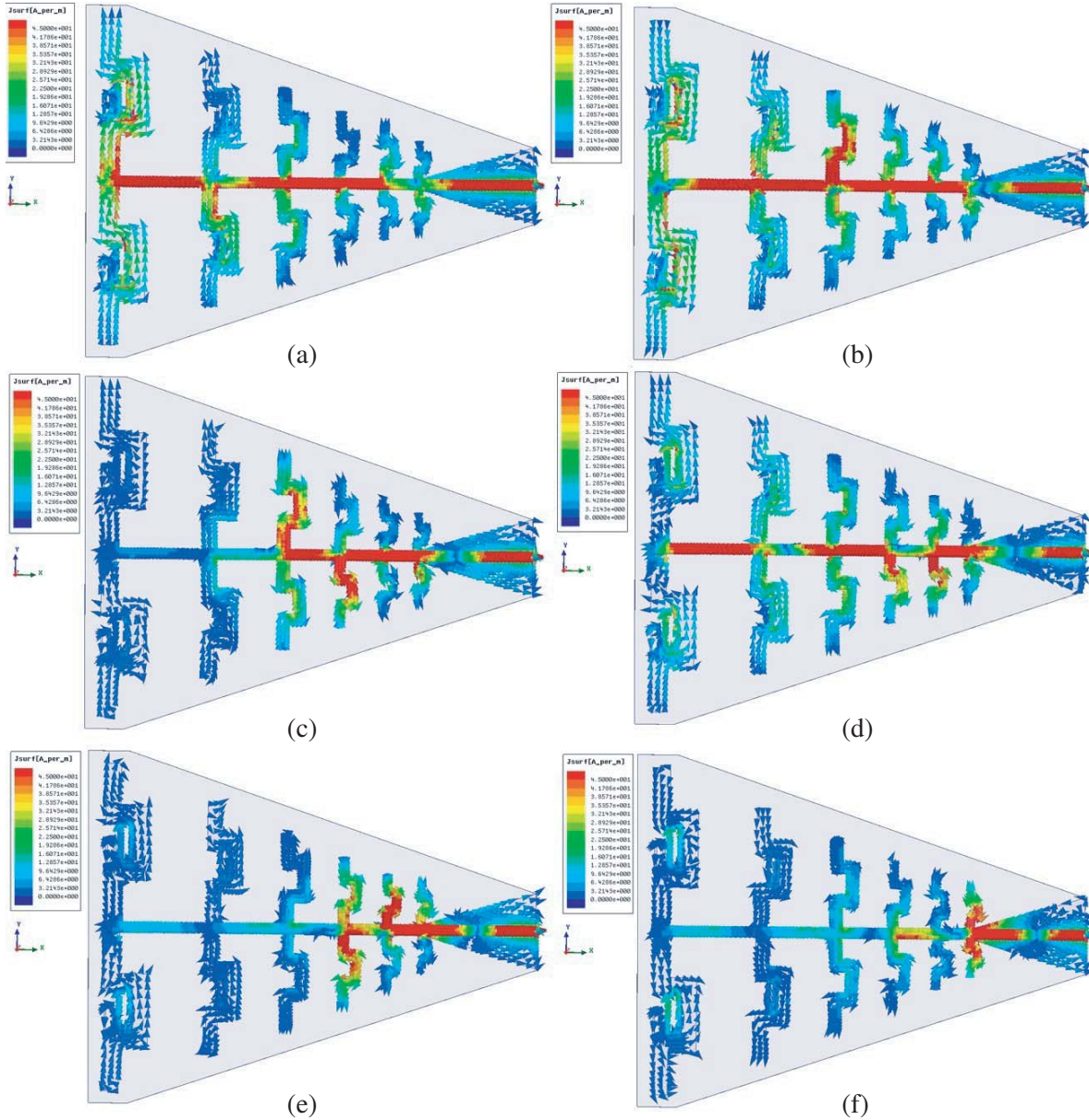
Figure 3. Surface current density of OSCDA antenna at (a) 1.2 GHz, (b) 1.501 GHz, (c) 1.93 GHz, (d) 2.198 GHz, (e) 2.6 GHz, (f) 3.014 GHz.

towards the apex (i.e., along the backfire direction) [28]. At any frequency, dipoles in the active region radiate, and other dipoles act as directors focusing the radiated field, making the radiation pattern directional [29]. For the sake of comparisons, the radiation patterns, in co and cross polarizations, both measured and simulated at three frequencies, viz., 1.501 GHz, 2.198 GHz, and 3.014 GHz, are shown in Figures 4(a)–(f). The antenna exhibits a stable radiation pattern over the range of frequencies, and the cross polarization levels are less than -15 dB at the frequencies of interest. The small variation in measured pattern from that of the simulated one is due to fabrication tolerances and inhomogeneities in the antenna substrate. Also the connector and coaxial cable are not included in simulation. In simulation, the antenna is fed by a differential port. So the effect of tapered feeding structure (which serves the purpose of a balun) is not reflected in simulation results, but is evident in measured results. Also the pattern is affected by the test environment and test fixture. The gain of OSCDA is measured using two antenna method inside an anechoic chamber. The peak gain is 10.3 dBi, at 3.3 GHz.
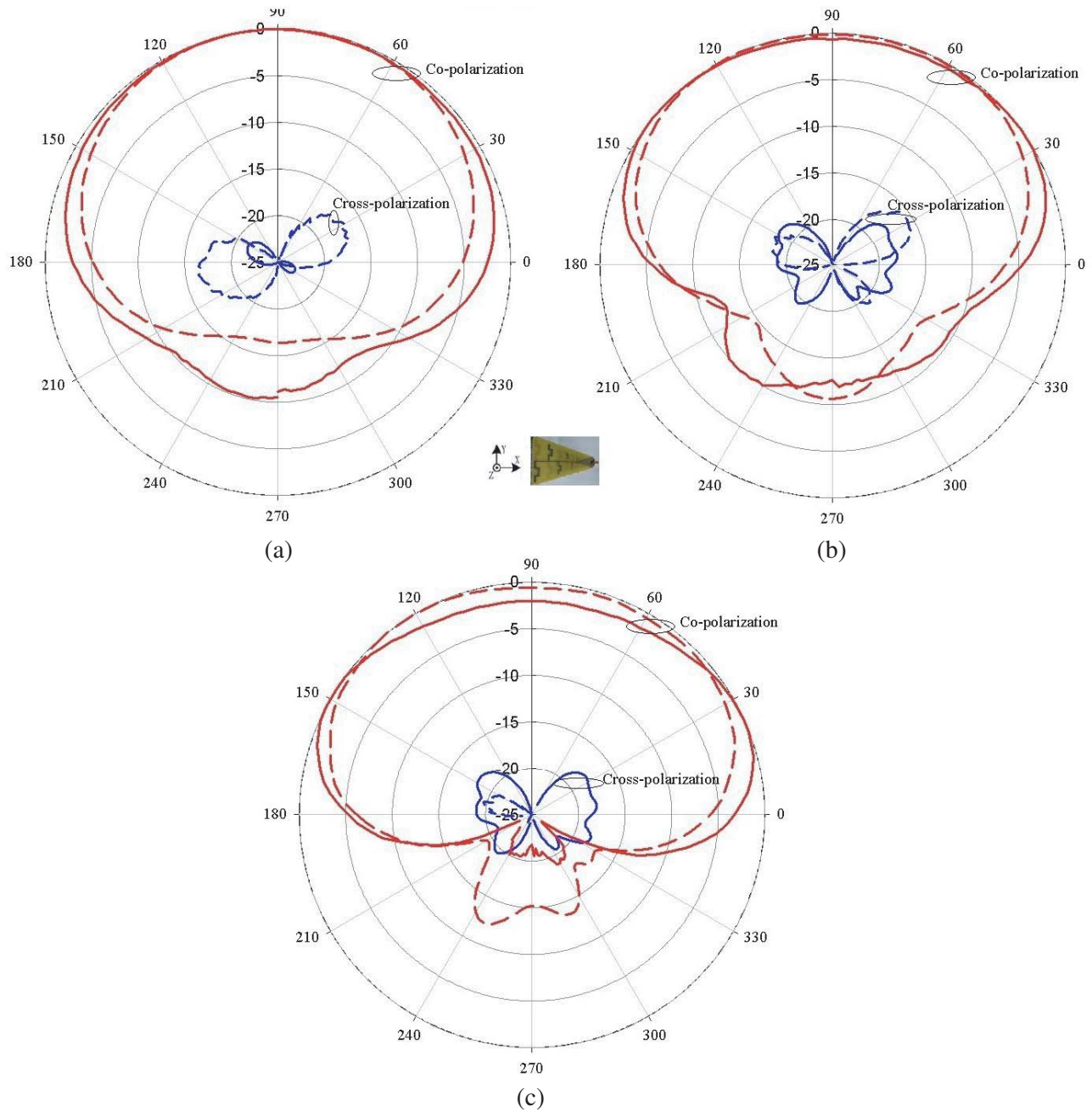
Figure 4. Normalized electric field patterns of OSCDA antenna in x-z plane, (a) at 1.501 GHz, (b) at 2.198 GHz, (c) at 3.014 GHz.

3. OSCDA AS LIQUID SENSOR

In this section, the capabilities of OSCDA sensor as generalized liquid sensor are assessed. Different cases studied include: (i) dilution of milk with water, (ii) adulteration of coconut oil with rice bran oil, (iii) adulteration of honey with sugar syrup, and (iv) varying concentration of salt and sugar in water. For the experiment, different samples with different adulteration levels (or concentration) are prepared. The samples are stirred after dilution and are allowed a time of approximately 5 minutes to reach equilibrium. The antenna is then immersed in the sample solution, as shown in Figure 5, and the reflection coefficient variation with frequency for each concentration is measured using N9923A FieldFox

Figure 5. Experimental setup for OSCDA as sensor.

Handheld RF Vector Network Analyzer. Measurements are taken at room temperature (25°C).

When the antenna is immersed in the test sample, the electromagnetic boundary conditions change. Due to dielectric perturbation phenomenon [24], the resonance frequency shifts. At resonance, there is strong current oscillation in the OLR's conducting loop. A strong electric field is produced at the gap (dimension of gap is approximately 0.001λ, where λ is the wavelength). This field is very sensitive to the dielectric placed close to the gap and produces change in resonant frequency. The response of liquid to electromagnetic radiation depends on the material properties, temperature, and chemical composition.

Liquids have complex permittivity ε given by [30]:

$$\varepsilon = \varepsilon' - j\varepsilon'' \tag{1}$$

where ε' is the real permittivity, and ε'' is the dielectric loss factor (or imaginary permittivity). ε' is related to capacitance and accounts for electric energy storage. ε'' accounts for the dielectric losses due to the conversion of electromagnetic energy to thermal energy. Both ε' and ε'' vary with frequency. Water is one of the main components of most liquid foods (example: milk, honey, etc.). Water is a polar molecule. Its permittivity is given by Debye relation given by [30]:

$$\varepsilon'(\omega) = \varepsilon'_\infty + \frac{\varepsilon'_S - \varepsilon'_\infty}{1 + \omega^2 \tau^2} \tag{2}$$

$$\varepsilon''(\omega) = \left(\frac{\varepsilon'_S - \varepsilon'_\infty}{1 + \omega^2 \tau^2} \right) \omega\tau \tag{3}$$

where ε'_S is the real static permittivity at low frequency; ε'_∞ is the real permittivity at very high frequency; and $\tau = 1/(2\pi f_R)$, f_R is the relaxation frequency, the frequency at which the imaginary part of the complex permittivity is maximum (i.e., maximum energy absorption).

3.1. Case Study (i): Dilution of Milk with Water

Milk is chosen for study because it is an important nutritional component and is easy to handle and prepare for the experiment. Six different samples of different dilutions are prepared by adding water

to milk. 0%, 20%, 40%, 60%, 80% and 100% solutions are prepared. 100% and 0% solutions refer to unadulterated milk and pure water, respectively. A 20% solution refers to a mixture of 200 ml of unadulterated milk and 800 ml of water.

The most important chemical component of milk is water. Apart from water, it contains ions and organic molecules such as proteins, carbohydrates, fats, and vitamins. The ions in milk are responsible for ionic conduction losses which are inversely proportional to the frequency. This loss factor is thus included in Equation (3). $\varepsilon''(\omega)$ is thus given by [30]:

$$\varepsilon''(\omega) = \left(\frac{\varepsilon'_S - \varepsilon'_\infty}{1 + \omega^2\tau^2} \right) \omega\tau + \frac{\sigma}{\omega\varepsilon_o} \tag{4}$$

Organic molecules in milk are associated with dipole moments. The various components of the milk interact with each other, which makes the scenario more complicated. Equations (2) and (4) are therefore only approximate. In general, ε' of pure milk decreases with frequency, and ε'' increases with frequency [30]. ε' of pure milk ranges from 70 to 75, and ε'' ranges from 5 to 10 at room temperature [30]. Also ε' increases with an increase in the water content in the solution [31]. Thus as dilution increases, the resonant frequency shifts to the lower side as can be seen from Figure 6. 100% solution (pure milk) is taken as a reference and corresponds to zero frequency shift. The resonance frequency, $f1$ (1.022 GHz), as seen from Figure 6 and Figure 7(a) shows maximum sensitivity to dilution.
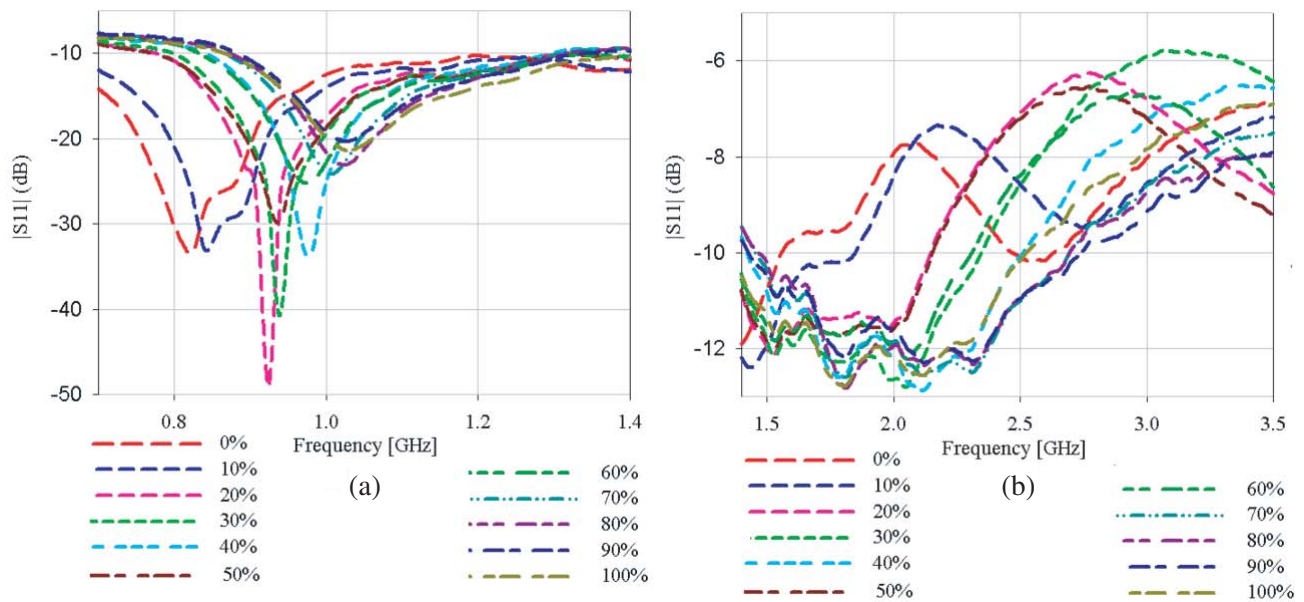

Figure 6. Sensing responses on different concentrations of milk.

The reflection coefficient increases with an increase in dilution as noted in Figure 7(b). In concentrated milk, the interaction between the constituent molecules, ions, and water is more. It means that there is less free water. Therefore, ionic conductivity is less, resulting in a lower ε'' and lower effective dielectric constant [17]. The load impedance is thus less in pure milk than that in free water. Thus reflection coefficient is minimal for pure milk. As dilution increases, free water molecules increase. Ionic conductivity and thus losses increase with dilution. Dielectric properties change due to interaction of dissolved ions and water molecules. Also there is less interaction between the organic molecules present. Thus the variation of reflection coefficient with concentration is nonlinear with dilution as seen from Figure 7(b). In general, the reflection coefficient increases with increase in dilution. There is also a change in Q factor, due to various dielectric losses associated with the material, which varies with dilution [32].
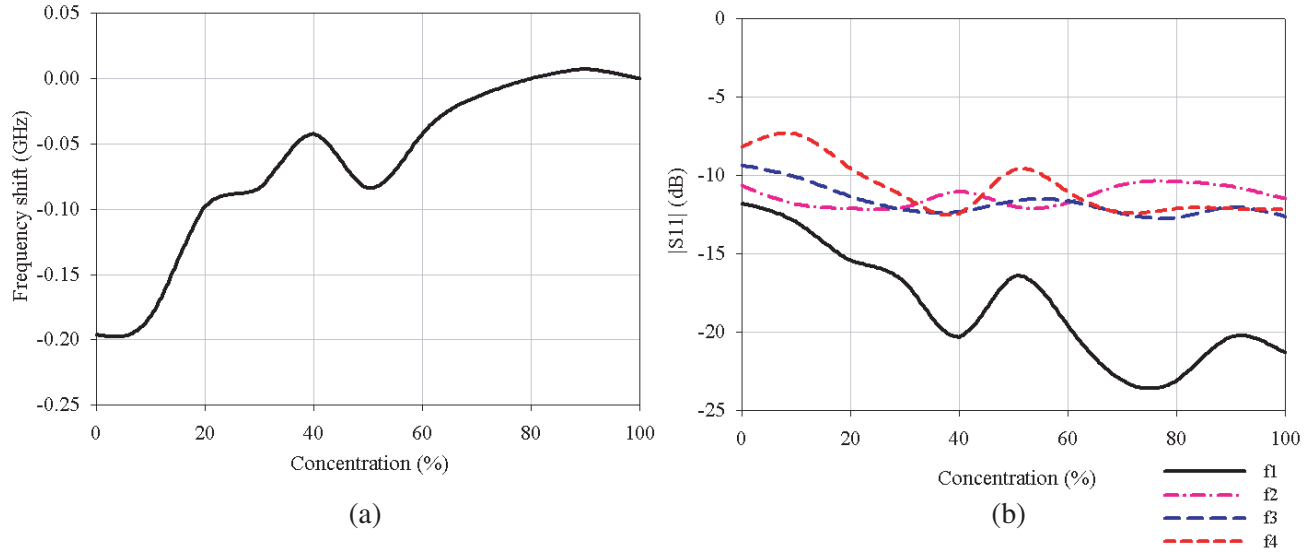
Figure 7. (a) Shift in resonant frequency ($f1$) taking pure milk (100% concentration) as reference. (b) Variation in reflection coefficient with varying concentration of milk at different frequencies $f1$ (1.022 GHz), $f2$ (1.512 GHz), $f3$ (1.834 GHz) and $f4$ (2.184 GHz).

3.2. Case Study (ii): Adulteration of Coconut Oil with Rice Bran Oil

Coconut oil is widely used for cooking and to prepare medicines. Coconut oil is adulterated with cheaper oils like rice bran oil, palm oil, etc. to increase profit. As a case study, coconut oil, is adulterated with rice bran oil. 12 samples of different adulteration levels (0%, 20%, 40%, 60%, 80%, 100%) are prepared. 100% refers to pure coconut oil. 0% refers to pure rice bran oil. A 20% sample has 200 ml coconut oil and 800 ml rice bran oil. The oils are mixed and allowed a time of 5 minutes to achieve equilibrium. It is also ensured that there are no air bubbles.

Edible vegetable oil is a mixture of unsaturated, saturated, and polyunsaturated fatty acids. The dielectric constant ε', is specific to an oil because it depends on the degree of saturation and the fatty acid composition. Coconut oil contains 82% saturated fatty acids, 6.3% monounsaturated fatty acids, and 1.7% polyunsaturated fatty acids. Major fatty acids present in coconut oil are lauric acid, myristic acid, palmitic acid, and caprylic acid. Rice bran oil contains 25% saturated fatty acids and 75% unsaturated fatty acids. Rice bran oil contains mainly oleic acid, linoleic acid and palmitic acid. Due to variation in composition and degree of saturation, these two oils have different ε'. Thus ε' and hence resonant frequencies are different for various edible oils, and thus are useful in differentiating them. Figure 8 shows how the resonant frequencies vary with different levels of adulteration. The resonant frequency $f5$ (2.628 GHz) shows maximum sensitivity to increase in percentage of adulteration levels. As the percentage of adulteration increases, the composition changes, also the degree of saturation. Thus, dielectric constant and loss factor change. ε' follows Debye relationship. ε' decreases from ε_0 to ε_∞ as the frequency increases. The loss factor ε'' also decreases with frequency, reaches a minimum, and then increases with frequency [33]. These effects are reflected in the variation in reflection coefficient and shift in resonant frequency as shown in Figures 8(a) and (b), respectively. As seen from Figure 8(b), the resonant frequency $f5$ (2.628 GHz) shows maximum sensitivity (frequency shift) to adulteration. Variation of reflection coefficient is nonlinear with frequency as can be seen from Figure 8(a).

3.3. Case Study (iii): Adulteration of Honey with Sugar Syrup

Honey is extracted from nectar and processed by honey bees. Due to immense health benefits, there is high market demand for pure honey. This has led to an increase in adulteration of honey for profit. Sugar syrup and other variants of sugar such as jaggery are added to pure honey. The adulterated honey
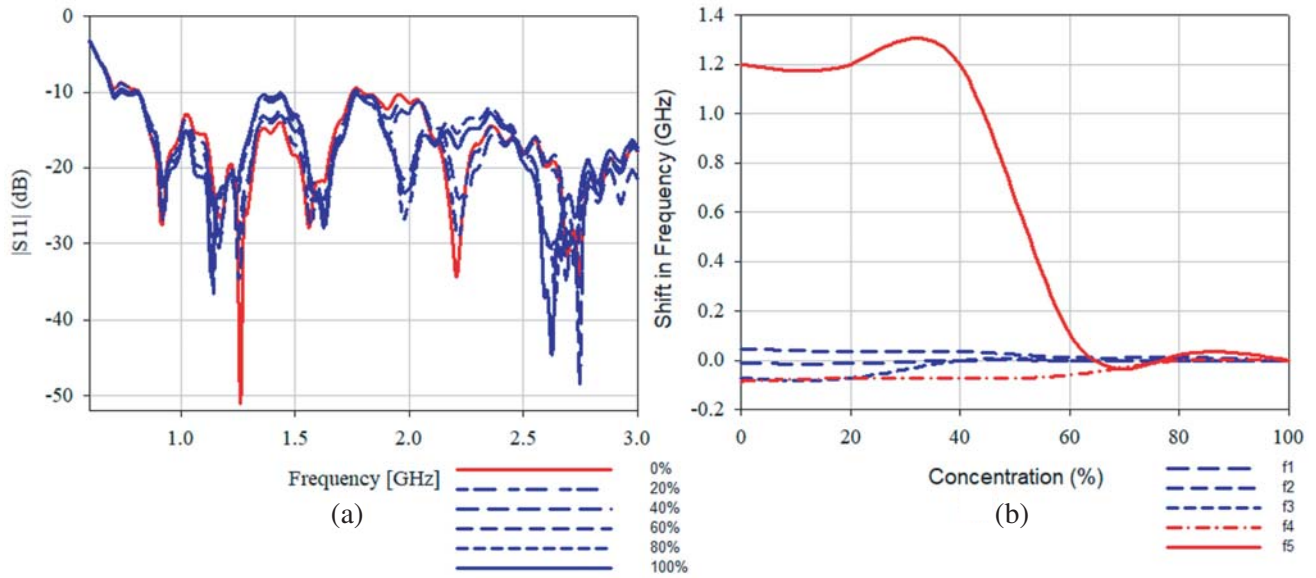
Figure 8. Sensing responses on different adulteration levels of coconut oil. (a) Variation of reflection coefficient with frequency. (b) Shift in resonant frequencies: $f1$ (0.924 GHz), $f2$ (1.28 GHz), $f3$ (1.632 GHz), $f4$ (1.98 GHz) and $f5$ (2.628 GHz) for different adulteration levels taking pure coconut oil as reference.

is very similar to the natural, pure honey, in appearance. So it is difficult to distinguish pure honey from adulterated ones. Here a simple antenna based experiment is presented to detect adulteration of honey with cane sugar syrup. For the experiment, six different samples of different dilutions of honey with cane sugar syrup are prepared by adding the adulterant to honey. 0%, 20%, 40%, 60%, 80%, and 100% mixtures are prepared. 100% and 0% mixture refer to pure honey and cane sugar syrup respectively. A 20% solution refers to a mixture of 200 ml of honey and 800 ml of cane sugar syrup.

Honey contains about 20% water, 78% sugar, and less than 0.25% ash. Among the sugars, there are 0–2% sucrose, 25.2–35.3% glucose, and 33.3–43% fructose. The dielectric properties of pure honey are given by the Davidson-Cole model [34]. The complex permittivity is given by [34]:

$$\varepsilon^*(\omega) = \varepsilon_\infty + \frac{\varepsilon_s - \varepsilon_\infty}{\left[1 + (j\omega\tau)^{1-\alpha}\right]^\beta} - j\frac{\sigma}{\omega\varepsilon_o} \tag{5}$$

where ω is the angular frequency, ε_s the static dielectric constant, τ the relaxation time, σ the dc conductivity, and α, β are the curve fitting parameters [34]. At room temperature, the dielectric constant (ε') and loss factor (ε'') of honey usually decrease with frequency. The dielectric parameters are influenced by the water content (W) and the total soluble solids content (S) of honey [35, 36]. The dielectric constant shows a linear relationship with W and S, and is given by [36]:

$$\varepsilon' = k_1 S + c_1 \tag{6}$$
$$\varepsilon' = k_2 W + c_2 \tag{7}$$

where k_1, k_2, c_1, c_2 are constants. For a given frequency, when the water content of honey increases, the dielectric constant increases, and the critical frequency of loss factor and the maximum loss factor move to the higher frequency side [36]. Also as the sucrose content increases, the dielectric constant and loss factor decrease. When honey is adulterated with sugar syrup, the water content and sucrose content increase. Thus the variation of ε' is nonlinear with levels of adulteration. In general, ε' increases with increase in adulteration. As ε' increases, the resonant frequency shifts to the lower side. Figure 9(b) shows that the resonant frequency shifts to the lower side as adulteration level increases. The frequency $f3$ (1.872 GHz) shows maximum sensitivity to adulteration with sugar syrup. The loss factor is related
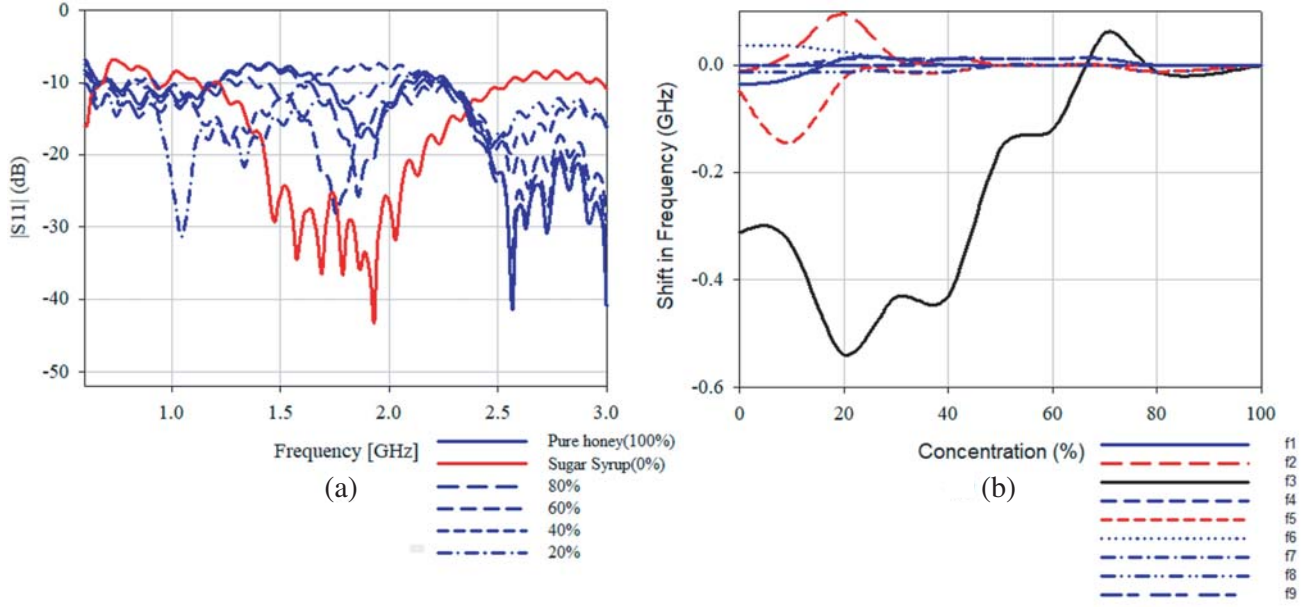
Figure 9. Sensing responses on different adulteration levels of honey. (a) Variation of reflection coefficient with frequency. (b) Shift in resonant frequencies: $f1$ (0.852 GHz), $f2$ (0.948 GHz), $f3$ (1.872 GHz), $f4$ (1.932 GHz), $f5$ (2.568 GHz), $f6$ (2.628 GHz), $f7$ (2.724 GHz), $f8$ (2.832 GHz), and $f9$ (2.916 GHz) for different adulteration levels, taking pure honey as reference.

to sucrose content (S_1) as [37]:

$$\varepsilon'' = S_1 a + b \tag{8}$$

where a and b are constants. As honey is adulterated with sugar syrup, the Q factor increases, due to decrease in loss factor and losses. This can be inferred from the variation in reflection coefficients shown in Figure 9(a).

3.4. Case Study (iv): Varying Concentration of Salt and Sugar in Water

A major cause of diseases is the contamination of food and water with harmful salt and sugar. Therefore, it is important to develop a cost-effective method for determining the salt and sugar content in food and water. As a proof of concept, readily available salt, sodium chloride (NaCl) and sugar, sucrose ($C_{12}H_{22}O_{11}$) are selected to prepare the samples for the experiment. For this experiment, salt/sugar is added and mixed with water to obtain a 1% to 20% salt/sugar solution.

It is noted that the reflection coefficient decreases with increase in concentration of salt as seen from Figure 10(a). This is because as the concentration increases, the free water molecules present in solution decrease. The dissolved ions form a bond with water molecules, resulting in reduced polarization, decreased ionic conductivity, and reduction in dielectric constant. Due to reduction in effective dielectric constant of the solution, the load impedance decreases. Thus the reflection coefficient increases with concentration of salt as seen from Figure 10(b).

Sucrose that molecule has a dipole moment. As the concentration of sugar increases, the dielectric properties of the solution change due to dipole-dipole interactions. Thus the reflection coefficient decreases with increase in percentage of sugar in solution as can be seen from Figure 11(a). The resonant frequency also varies for different concentration levels as can be seen from Figure 11(b). As the concentration of sugar in solution increases, dipole-dipole interaction is more. Thus dielectric constant and Q factor vary. As concentration increases, there are less free water molecules because sugar molecules form a bond with water molecules. Thus the shift in resonant frequency as seen from Figure 11(b) is nonlinear.
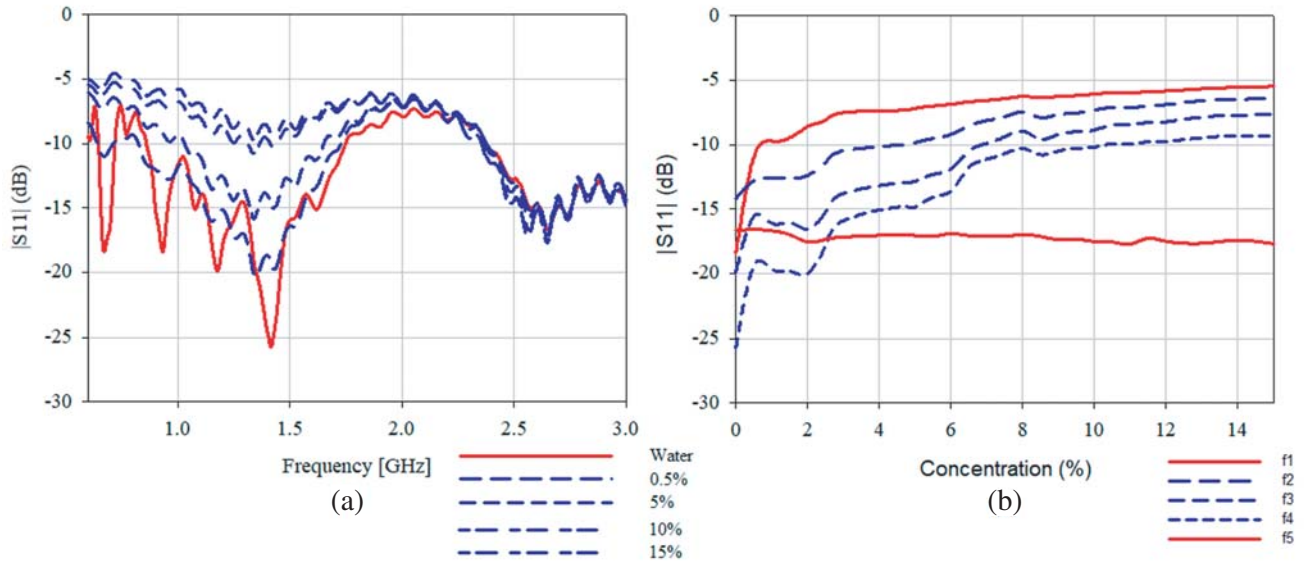
Figure 10. Sensing responses on different concentration levels of salt. (a) Variation of reflection coefficient with frequency. (b) Reflection coefficient at resonant frequencies: $f1$ (0.672 GHz), $f2$ (0.96 GHz), $f3$ (1.176 GHz), $f4$ (1.416 GHz) and $f5$ (2.652 GHz) for different adulteration levels taking water as reference.
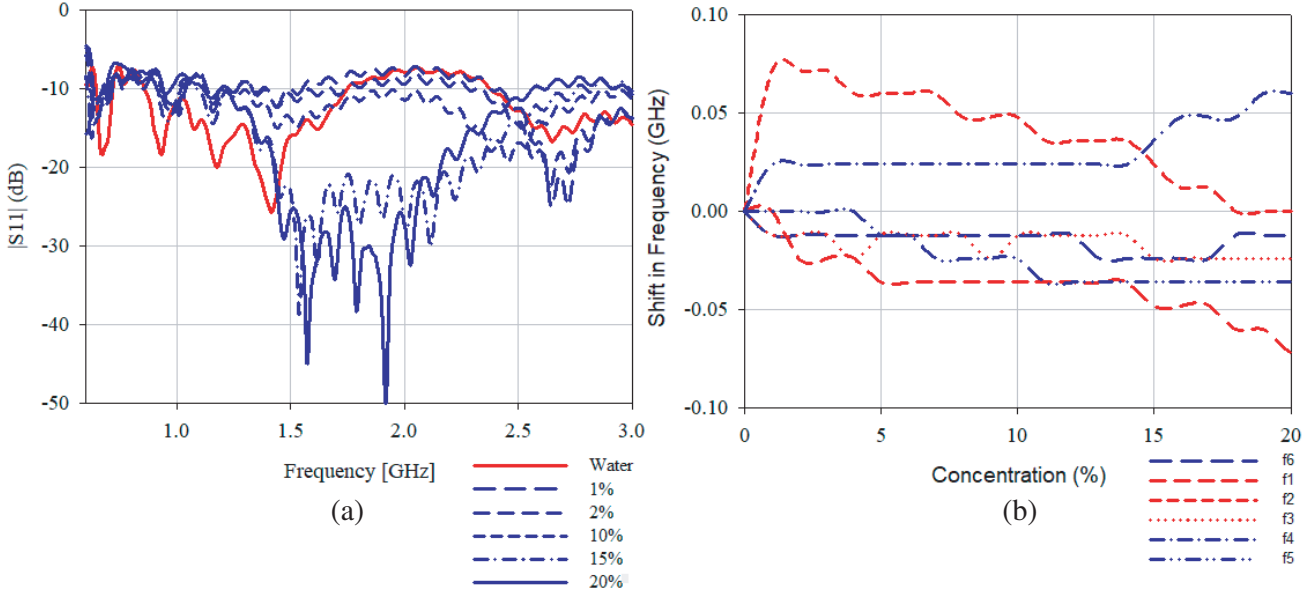

Figure 11. Sensing responses on different concentration levels of sugar (a) Variation of reflection coefficient with frequency (b) Reflection coefficient at resonant frequencies: $f1$ (0.672 GHz), $f2$ (0.936 GHz), $f3$ (1.176 GHz), $f4$ (1.416 GHz), $f5$ (2.652 GHz) and $f6$ (2.736 GHz) for different adulteration levels taking water as reference.

4. CONCLUSION

A novel sensor for detecting the contaminations has been presented, fabricated, and experimentally assessed. The antenna is fabricated on a substrate with relative permittivity 4.4. The antenna consists of an array of dipoles which are bent and to which OLRs have been added. The antenna does not require an external balun. The antenna is therefore compact and easy to fabricate. The antenna performances in terms of VSWR, beam pattern, and gain are quite satisfactory. The measured reflection coefficient in solution of different case studies shows that the reflection coefficient variation with frequency is typical of a liquid and can be used to identify adulteration. Experiments show that the antenna-based sensor has a reasonably good sensitivity to detect adulteration in liquids and is a cheap, but effective solution for food quality assessment applications. To improve the reliability of the device, more experiments are needed. For example, it is necessary to study different varieties of honey, milk, etc. and characterize and calibrate the device based on the results. To accommodate more varieties of liquids with different optical properties, using the same design principle, antenna can be designed for a wider bandwidth or higher frequencies to detect the adulteration of the liquid. The idea presented in the paper is only a proof of concept.

ACKNOWLEDGMENT

REFERENCES

1. Lee, C., W. Wang, B. K. Wilson, M. Connett, and M. D. Keller, "Detecting adulterants in milk with lower cost mid-infrared and raman spectroscopy," *Optics and Biophotonics in Low-Resource Settings IV*, Vol. 10485, 104850F, International Society for Optics and Photonics, 2018.

2. Bogdanov, S. and P. Martin, "Honey authenticity," *Mitteilungen aus Lebensmitteluntersuchung und Hygiene*, Vol. 93, No. 3, 232–254, 2002.

3. Mai, Z., B. Lai, M. Sun, J. Shao, and L. Guo, "Food adulteration and traceability tests using stable carbon isotope technologies," *Tropical Journal of Pharmaceutical Research*, Vol. 18, No. 8, 2019.

4. Cabanero, A. I., J. L. Recio, and M. Ruperez, "Liquid chromatography coupled to isotope ratio mass spectrometry: A new perspective on honey adulteration detection," *Journal of Agricultural and Food Chemistry*, Vol. 54, No. 26, 9719–9727, 2006.

5. Pérez, R. A., C. Sánchez-Brunete, R. M. Calvo, and J. L. Tadeo, "Analysis of volatiles from spanish honeys by solid-phase microextraction and gas chromatography-mass spectrometry," *Journal of Agricultural and Food Chemistry*, Vol. 50, No. 9, 2633–2637, 2002.

6. Ulloa, P. A., R. Guerra, A. M. Cavaco, A. M. R. Da Costa, A. C. Figueira, and A. F. Brigas, "Determination of the botanical origin of honey by sensor fusion of impedance e-tongue and optical spectroscopy," *Computers and Electronics in Agriculture*, Vol. 94, 1–11, 2013.

7. Subari, N., J. M. Saleh, A. M. Shakaff, and A. Zakaria, "A hybrid sensing approach for pure and adulterated honey classification," *Sensors*, Vol. 12, No. 10, 14022–14040, 2012.

8. Arroyo Negrete, M. A., K. Wrobel, F. J. Acevedo Aguilar, E. Yanez Barrientos, A. R. Corrales Escobosa, and K. Wrobel, "Determination of fatty acid methyl esters in cosmetic castor oils by flow injection — electrospray ionization — high-resolution mass spectrometry," *International Journal of Cosmetic Science*, Vol. 40, No. 3, 295–302, 2018.

9. Escuderos, M. E., S. Sánchez, and A. Jiménez, "Quartz Crystal Microbalance (QCM) sensor arrays selection for olive oil sensory evaluation," *Food Chemistry*, Vol. 124, No. 3, 857–862, 2011.

10. Fang, G., J. Y. Goh, M. Tay, H. F. Lau, and S. F. Yau Li, "Characterization of oils and fats by 1h nmr and gc/ms fingerprinting: Classification, prediction and detection of adulteration," *Food Chemistry*, Vol. 138, No. 2–3, 1461–1469, 2013.

11. H. L. Gan, Y. B. Che Man, C. P. Tan, I. Nor Aini, and S. A. H. Nazimah, "Characterisation of vegetable oils by surface acoustic wave sensing electronic nose," *Food Chemistry*, Vol. 89, No. 4, 507–518, 2005.

12. Apetrei, I. M. and C. Apetrei, "Detection of virgin olive oil adulteration using a voltammetric e-tongue," *Computers and Electronics in Agriculture*, Vol. 108, 148–154, 2014.

13. Chakraborti, H., S. Sinha, S. Ghosh, and S. K. Pal, "Interfacing water soluble nanomaterials with uorescence chemosensing: Graphene quantum dot to detect hg2+ in 100% aqueous solution," *Materials Letters*, Vol. 97, 78–80, 2013.

14. Jain, S., P. K. Mishra, V. V. Thakare, and J. Mishra, "Microstrip moisture sensor based on microstrip patch antenna," *Progress In Electromagnetics Research M*, Vol. 76, 177–185, 2018.

15. Fernandez-Salmeron, J., A. Rivadeneyra, M. A. Carvajal Rodríguez, L. F. Capitan-Vallvey, and A. J. Palma, "HF RFID tag as humidity sensor: Two different approaches," *IEEE Sensors Journal*, Vol. 15, No. 10, 5726–5733, 2015.

16. Saadat, W., S. A. Raurale, G. A. Conway, and J. McAllister, "User identification through wearable antenna characteristics at 2.45 GHz," *12th European Conference on Antennas and Propagation (EuCAP 2018)*, 2018.

17. Islam, M. T., M. N. Rahman, M. S. J. Singh, and M. Samsuzzaman, "Detection of salt and sugar contents in water on the basis of dielectric properties using microstrip antenna-based sensor," *IEEE Access*, Vol. 6, 4118–4126, 2018.

18. Salim, A. and S. Lim, "Review of recent metamaterial micro uidic sensors," *Sensors*, Vol. 18, No. 1, 232, 2018.

19. Lu, F., Q. Tan, Y. Ji, Q. Guo, Y. Guo, and J. Xiong, "A novel metamaterial inspired high-temperature microwave sensor in harsh environments," *Sensors*, Vol. 18, No. 9, 2879, 2018.

20. Bui, T. S., T. D. Dao, L. H. Dang, L. D. Vu, A. Ohi, T. Nabatame, Y. P. Lee, T. Nagao, and C. V. Hoang, "Metamaterial-enhanced vibrational absorption spectroscopy for the detection of protein molecules," *Scientific Reports*, Vol. 6, 32123, 2016.

21. Ebrahimi, A., W. Withayachumnankul, S. Al-Sarawi, and D. Abbott, "High-sensitivity metamaterial-inspired sensor for microfluidic dielectric characterization," *IEEE Sensors Journal*, Vol. 14, No. 5, 1345–1351, 2013.

22. Perez, M. D., G. Thomas, S. R. M. Shah, J. Velander, N. B. Asan, P. Mathur, M. Nasir, D. Nowinski, D. Kurup, and R. Augustine, "Preliminary study on microwave sensor for bone healing follow-up after cranial surgery in newborns," *12th European Conference on Antennas and Propagation (EuCAP 2018)*, 2018.

23. Shah, S. R. M., J. Velander, P. Mathur, M. D. Perez, N. B. Asan, D. G. Kurup, T. Blokhuis, and R. Augustine, "Penetration depth evaluation of split ring resonator sensor using in-vivo microwave reflectivity and ultrasound measurements," *12th European Conference on Antennas and Propagation (EuCAP 2018)*, 2018.

24. Wongkasem, N. and M. Ruiz, "Multi-negative index band metamaterial-inspired microfluidic sensors," *Progress In Electromagnetics Research C*, Vol. 94, 29–41, 2019.

25. Rajendran, J. and S. K. Menon, "On the miniaturization of log periodic koch dipole antenna using split ring resonators," *Progress In Electromagnetics Research Letters*, Vol. 63, 107–113, 2016.

26. Casula, G. A., P. Maxia, G. Mazzarella, and G. Montisci, "Design of a printed log-periodic dipole array for ultra-wideband applications," *Progress In Electromagnetics Research C*, Vol. 38, 15–26, 2013.

27. Saurav, K., D. Sarkar, and K. V. Srivastava, "Dual-band circularly polarized cavity-backed crossed-dipole antennas," *IEEE Antennas and Wireless Propagation Letters*, Vol. 14, 52–55, 2014.

28. Abdo-Sánchez, E., J. Esteban, T. M. Martin-Guerrero, C. Camacho-Penalosa, and P. S. Hall, "A novel planar log-periodic array based on the wideband complementary strip-slot element," *IEEE Transactions on Antennas and Propagation*, Vol. 62, No. 11, 5572–5580, 2014.

29. Carrel, R., "The design of log-periodic dipole antennas," *1958 IRE International Convention Record*, Vol. 9, 61–75, IEEE, 1966.

30. Nunes, A. C., X. Bohigas, and J. Tejada, "Dielectric study of milk for frequencies between 1 and 20 GHz," *Journal of Food Engineering*, Vol. 76, No. 2, 250–255, 2006.

31. Barbosa-Cánovas, G. V., *EOLSS: Food Engineering*, United Nations Educational, 2005.

32. Chuma, E. L., Y. Iano, G. Fontgalland, and L. L. B. Roger, "Microwave sensor for liquid dielectric characterization based on metamaterial complementary split ring resonator," *IEEE Sensors Journal*, Vol. 18, No. 24, 9978–9983, 2018.

33. Hu, L., K. Toyoda, and I. Ihara, "Dielectric properties of edible oils and fatty acids as a function of frequency, temperature, moisture and composition," *Journal of Food Engineering*, Vol. 88, No. 2, 151–158, 2008.

34. Puranik, S., A. Kumbharkhane, and S. Mehrotra, "Dielectric properties of honey-water mixtures between 10 MHz to 10 GHz using time domain technique," *Journal of Microwave Power and Electromagnetic Energy*, Vol. 26, No. 4, 196–201, 1991.

35. Ahmed, J., S. T. Prabhu, G. S. V. Raghavan, and M. Ngadi, "Physico-chemical, rheological, calorimetric and dielectric behavior of selected indian honey," *Journal of Food Engineering*, Vol. 79, No. 4, 1207–1213, 2007.

36. Guo, W., X. Zhu, Y. Liu, and H. Zhuang, "Sugar and water contents of honey with dielectric property sensing," *Journal of Food Engineering*, Vol. 97, No. 2, 275–281, 2010.

37. Guo, W., Y. Liu, X. Zhu, and S. Wang, "Dielectric properties of honey adulterated with sucrose syrup," *Journal of Food Engineering*, Vol. 107, No. 1, 1–7, 2011.